

Simplicial models of social contagion

Iacopo Iacopini^{1,2}, Giovanni Petri^{3,4}, Alain Barrat^{5,3} & Vito Latora^{1,2,6,7}

¹*School of Mathematical Sciences, Queen Mary University of London, London E1 4NS, United Kingdom*

²*The Alan Turing Institute, The British Library, London NW1 2DB, United Kingdom*

³*ISI Foundation, Via Chisola 5, 10126 Turin, Italy*

⁴*ISI Global Science Foundation, 33 W 42nd St 10036 New York NY, United States*

⁵*Aix Marseille Univ, Université de Toulon, CNRS, CPT, Marseille, France*

⁶*Dipartimento di Fisica ed Astronomia, Università di Catania and INFN, I-95123 Catania, Italy*

⁷*Complexity Science Hub Vienna (CSHV), Vienna, Austria*

Complex networks have been successfully used to describe the spreading of diseases in populations of interacting individuals. Conversely, pairwise interactions are often not enough to characterize processes of social contagion, such as opinion formation or the adoption of novelties, where more complex dynamics of peer influence and reinforcement mechanisms are at work. Here we introduce a higher-order model of social contagion in which a social system is represented by a simplicial complex and the contagion can occur, with different transmission rates, not only over the links but also through interactions in groups of different sizes. Numerical simulations of the model on both empirical data and synthetic simplicial complexes highlight the emergence of novel phenomena such as a discontinuous transition induced by higher-order interactions. We show analytically that the transition is discontinuous with the formation of a bistable region where healthy and endemic states co-exist. Our results help explain why critical masses are required to initiate social changes, and contribute to the understanding of the role of higher-order interactions in complex systems.

Introduction

Complex networks describe well the connectivity of systems of various nature ^{1,2} and are widely used as the underlying – and possibly multilayered ³– social structure on which dynamical processes ^{4,5}, such as disease spreading ⁶, diffusion and adoption of innovation ^{7–9}, and opinion formation ¹⁰ occur. For example, when modeling an epidemic spreading in a population ⁶, the transmission between infectious and healthy individuals is typically assumed: *(i)* to occur through pairwise interactions between infectious and healthy individuals, and *(ii)* to be caused even by a single exposure of a healthy individual to an infectious one. Such processes of *simple contagion* can be conveniently represented by transmission mechanisms along the links of the network of contacts between individuals.

When dealing instead with social contagion phenomena, such as the adoption of norms, behaviours or new products, or the diffusion of rumors or fads, the situation is more complex. Simple epidemic-like contagion can suffice to describe some cases, such as easily convincing rumors or domino effects ¹¹. In other situations, however, they do not provide a satisfactory description, especially in those cases where more complex dynamics of peer influence and reinforcement mechanisms are at work ¹². *Complex contagion* mechanisms have been proposed to account for these effects. As defined by Centola & Macy ¹¹: “a contagion is complex if its transmission requires an individual to have contact with two or more sources of activation”, i.e. if a “contact with a single active neighbor is not enough to trigger adoption”. Complex contagion can hence be broadly defined as a process in which exposure to multiple sources presenting the same stimulus is needed for

the contagion to occur. Empirical evidence that contagion processes including multiple exposure can be needed to describe social contagion has been provided in various contexts and experiments^{13–17}.

Modeling of social contagion processes has been driven by these considerations in several directions. Threshold models assume that, in order to adopt a novel behavior, an individual needs to be convinced by a fraction of his/her social contacts larger than a given threshold^{11,16,18–21}. The processes considered in such models are usually deterministic. Another modeling framework for social contagion relies instead on generalizations of epidemic-like processes, with stochastic contagion processes whose rates might depend on the number of sources of exposure to which an individual is linked to, i.e., with a complex contagion flavor^{15,21–26}. All these models are however still defined on networks of interactions between individuals: even when multiple interactions are needed for a contagion to take place, in both threshold and epidemic-like models, the fundamental building blocks of the system are pairwise interactions, structurally represented by the links of the network on which the process is taking place.

Here, we propose to go further and take into account that contagion can occur in different ways, either through pairwise interactions (the links of a network) or through group interactions, i.e. through higher-order structures. Indeed, while an individual can be convinced independently by each of his/her neighbors (simple contagion), or by the successive exposure to the arguments of different neighbors (complex contagion), a fundamentally different mechanism is at work if the neighbors of an individual convince him/her *in a group interaction*. For example, we can adopt a

new norm because of two-body processes, which means we can get convinced, separately, by each one of our first neighbors in our social network who have already adopted the norm. However, this is qualitatively different from a mechanism of contagion in which we get convinced because we are part of a social group of three individuals, and our two neighbors are both adopters. In this case the contagion is a three-body process that mimics the simplest multiple source of reinforcement that induces adoption. The same argument can easily be generalized to larger group sizes.

Simplicial representations are then more suited than networks to describe the co-existence of pairwise and higher-order interactions, as they characterize efficiently interactions between more than two units^{27,28}. The model of *simplicial contagion* proposed here is thus an epidemic-like model of social contagion on simplicial complexes, which takes into account the fact that the processes and their rates can differ, depending on whether a contagion occurs through a link or is due to a group interaction. Overall, our model combines stochastic processes of simple contagion (pairwise interactions) and of complex contagion occurring through group interactions in which an individual is simultaneously exposed to multiple sources of contagion.

To build such a modeling framework, we formalise a social group as a simplex, and we adopt simplicial complexes as the underlying structure of the social system under consideration (see Figure 1a-b). We recall that, in its most basic definition, a k -simplex σ is a set of $k + 1$ vertices $\sigma = [p_0, \dots, p_k]$. It is then easy to see the difference between a group interaction among three elements, which can be represented as a 2-simplex or “full” triangle $[p_0, p_1, p_2]$, and the collection of its edges, $[p_0, p_1], [p_0, p_2], [p_1, p_2]$. Just like a collection of edges defines a network, a collection

of simplices defines a simplicial complex. Formally, a simplicial complex \mathcal{K} on a given set of vertices \mathcal{V} , with $|\mathcal{V}| = N$, is a collection of simplices, with the extra requirement that if simplex $\sigma \in \mathcal{K}$, then all the sub-simplices $\nu \subset \sigma$ built from subsets of σ are also contained in \mathcal{K} . Such a requirement, which makes simplicial complexes a special type of hypergraphs (see Supplementary Note 4), seems appropriate in the definition of higher-dimensional groups in the context of social systems, and simplicial complexes have indeed been used to represent social aggregation in human communication ²⁹. Removing this extra requirement would imply, for instance, modelling a group interaction of three individuals without taking into account also the dyadic interactions among them. The same argument can be extended to interactions of four or more individuals: it is reasonable to assume that the existence of high-order interactions implies the presence of the lower-order interactions. For simplicity and coherence with the standard network nomenclature, we call nodes (or vertices) the 0-simplices and links (or edges) the 1-simplices of a simplicial complex \mathcal{K} , while 2-simplices correspond to the (“full”) triangles, 3-simplices to the tetrahedra of \mathcal{K} , and so on (see Figure 1a). Simplicial complexes, differently from networks, can thus efficiently characterize interactions between any number of units. Simplicial complexes are not a new idea ³⁰, but the interest in them has been renewed ^{28,31} thanks to the availability of new data sets and of recent advances in topological data analysis techniques ³². In particular, they recently proved to be useful in describing the architecture of complex networks ^{33–35} functional ^{36–38} and structural brain networks ³⁹, protein interactions ⁴⁰, semantic networks ⁴¹, and co-authorship networks in science ⁴².

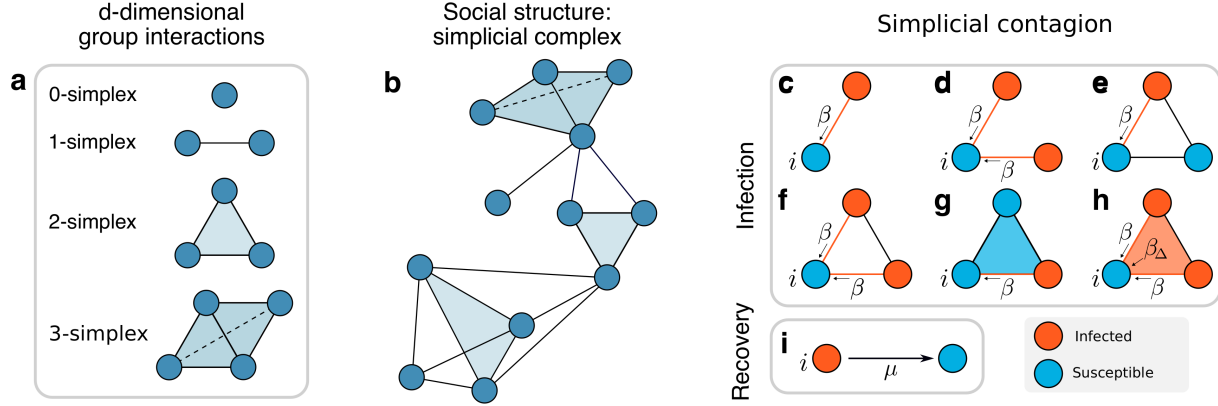


Figure 1: **Simplicial Contagion Model (SCM)**. The underlying structure of a social system is made of simplices, representing d -dimensional group interactions **(a)**, organized in a simplicial complex **(b)**. **c-h** Different channels of infection for a susceptible node i in the Simplicial Contagion Model (SCM) of order $D = 2$. Susceptible and infected nodes are colored in blue and red, respectively. Node i is in contact with one **(c, e)** or more **(d, f)** infected nodes through links (1-simplices), and it becomes infected with probability β at each timestep through each of these links. **g-h** Node i belongs to a 2-simplex (triangle). In **g** one of the nodes of the 2-simplex is not infected, so i can only receive the infection from the (red) link, with probability β . In **h** the two other nodes of the 2-simplex are infected, so i can get the infection from each of the two 1-faces (links) of the simplex with probability β , and also from the 2-face with probability $\beta_2 = \beta_\Delta$. **i** Infected nodes recover with probability μ at each timestep, as in the standard SIS model.

Results

The contagion model. In order to model a simplicial contagion process, we associate a dynamical binary state variable x to each of the N vertices of \mathcal{K} , such that $x_i(t) \in \{0, 1\}$ represents the state of vertex i at time t . Using a standard notation, we divide the population of individuals into two classes of susceptible (S) and infectious (I) nodes, corresponding respectively to the values 0 and 1 of the state variable x . In the context of adoption processes, the state I represents individuals who have adopted a behaviour. At each time t , the macroscopic order parameter is given by the density of infectious nodes $\rho(t) = \frac{1}{N} \sum_{i=1}^N x_i(t)$. The model we propose here, the so-called *Simplicial Contagion Model (SCM) of order D* , with $D \in [1, N - 1]$, is governed by a set of D control parameters $B = \{\beta_1, \beta_2, \dots, \beta_D\}$, whose elements represent the probability per unit time for a susceptible node i that participates to a simplex σ of dimension D to get the infection from each one of the subfaces composing σ , under the condition that all the other nodes of the subface are infectious. In practice, with this notation, β_1 is equal to the standard probability of infection β that a susceptible node i gets the infection from an infected neighbor j through the link (i, j) (corresponding to the process $S + I \rightarrow 2I$). Similarly, the second parameter $\beta_2 \equiv \beta_\Delta$ corresponds to the probability per unit time that node i receives the infection from a “full” triangle (2-simplex) (i, j, k) in which both j and k are infectious, $\beta_3 = \beta_{\boxtimes}$ from a group of size 4 (3-simplex) to which it belongs, and so on. Such processes can be represented as $Simp(S, nI) \rightarrow Simp((n + 1)I)$: a susceptible node, part of a simplex of $n + 1$ nodes among which all other n nodes are infectious, becomes infectious with probability per unit time β_n . Thanks to the simplicial complex requirements that all subsimplices of a simplex are included, contagion processes in a n -

simplex among which $p < n$ nodes are infectious are also automatically considered, each of the $n + 1 - p$ susceptible nodes being in a simplex of size $p + 1$ with the p infectious ones. Notice, however, that this assumption can be dropped and the contagion model extended to the case of hypergraphs^{43,44} (see Supplementary Note 4). Figure 1c-h illustrates the concrete example of the six possible ways in which a susceptible node i can undergo social contagion for an SCM of order $D = 2$ with parameters β and β_{Δ} . Finally, the recovery dynamics ($I \rightarrow S$) is controlled by the node-independent recovery probability μ (Figure 1i). Notice that the SCM of order D reduces to the standard SIS model on a network when $D = 1$, since in this case the infection can only be transmitted through the links of \mathcal{K} .

Simplicial contagion on real-world simplicial complexes. To explore the phenomenology of the simplicial contagion model, we first consider its evolution on empirical social structures. To this aim, we consider publicly available data sets describing face-to-face interactions collected by the SocioPatterns collaboration⁴⁵. Face-to-face interactions represent indeed a typical example in which group encounters are fundamentally different from sets of binary interactions and can naturally be encoded as simplices. The time-resolved nature of the data allows us to create simplicial complexes describing the aggregated social structure, as described in Methods. For simplicity, we only consider simplices of dimension up to $D = 2$. We consider data on interactions collected in four different social contexts: a workplace, a conference, a hospital and a high school (see Methods for details on the data sets).

We simulate the SCM over the simplicial complexes obtained from the four data sets as

described in Methods. In particular, we start with an initial density ρ_0 of infectious nodes and we run the simulations by taking into consideration all the possible channels of infection illustrated in Figure 1c-h. We stop a simulation if an absorbing state is reached, otherwise we compute the average stationary density of infectious nodes ρ^* by averaging the values measured in the last 100 time-steps after reaching a stationary state. The results are averaged over 120 runs obtained with randomly placed initial infectious nodes with the same density ρ_0 . Moreover, the different data sets correspond to different densities of 1- and 2-simplices (see Supplementary Note 1). We thus rescale the infectivity parameters β and β_Δ respectively by the average degree $\langle k \rangle$ and by the average number of 2-simplices incident on a node, $\langle k_\Delta \rangle$. We finally express all results as functions of the rescaled parameters $\lambda = \beta \langle k \rangle / \mu$ and $\lambda_\Delta = \beta_\Delta \langle k_\Delta \rangle / \mu$.

Figure 2 shows the resulting prevalence curves for the four data sets (see also Supplementary Note 5). In each panel (b,d,f,h), the average fraction of infected nodes ρ^* in the stationary state is plotted as a function of the rescaled infectivity $\lambda = \beta \langle k \rangle / \mu$ for simulations of the SCM with $\lambda_\Delta = 0.8$ (black triangles) and $\lambda_\Delta = 2$ (orange squares). For comparison, we also plot the case $\lambda_\Delta = 0$, which is equivalent to the standard SIS model with no higher-order effects (blue circles). We observe two radically different behaviours for the two values of $\lambda_\Delta \neq 0$. For $\lambda_\Delta = 0.8$, the density of infectious nodes varies as a function of λ in a very similar way to the case $\lambda_\Delta = 0$ (simple contagion), with a continuous transition. For $\lambda_\Delta = 2$ we observe instead the appearance of an endemic state with $\rho^* > 0$ at a value of λ^c well below the epidemic threshold of the other two cases. Furthermore, this transition appears to be discontinuous, and an hysteresis loop appears in a bi-stable region, where both healthy $\rho^* = 0$ and endemic $\rho^* > 0$ states can co-exist (dashed

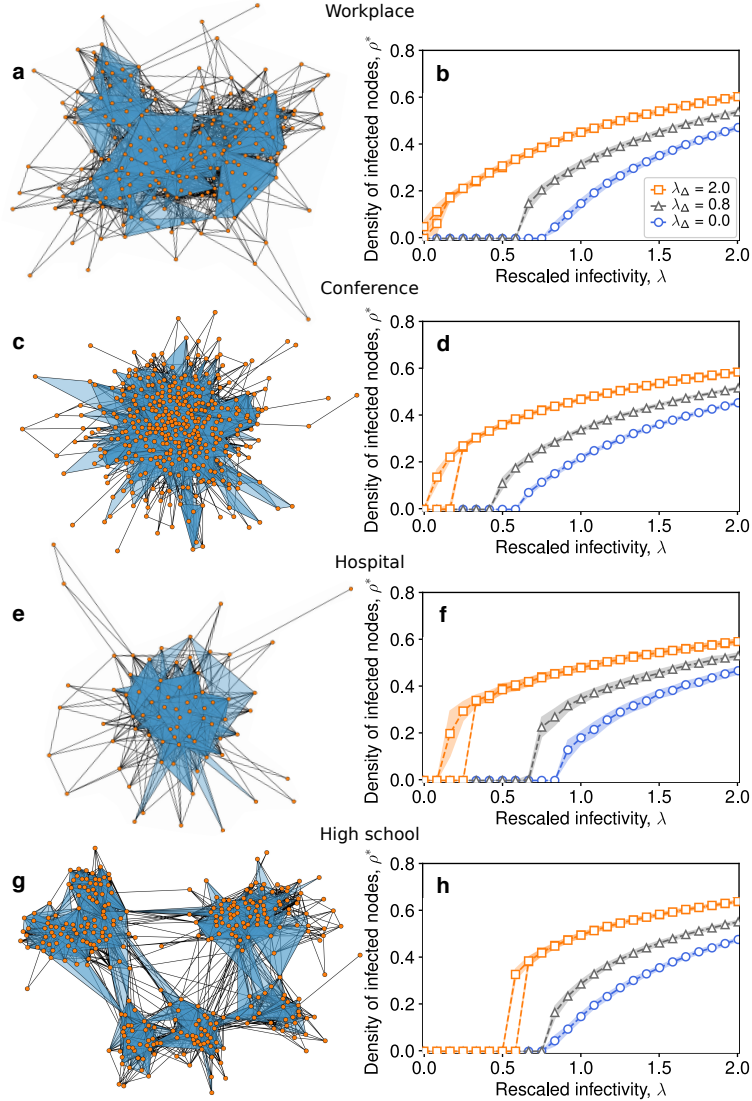


Figure 2: **SCM of order $D = 2$ on real world higher-order social structures.** Simplicial complexes are constructed from high-resolution face-to-face contact data recorded in four different context: **a** a workplace, **c** a conference, **e** a hospital and **g** a high school. Prevalence curves are respectively reported in panels **b**, **d**, **f** and **h**, in which the average fraction of infectious nodes obtained in the numerical simulations is plotted against the rescaled infectivity $\lambda = \beta \langle k \rangle / \mu$ for different values of the rescaled parameter $\lambda_\Delta = \beta_\Delta \langle k_\Delta \rangle / \mu$, namely $\lambda_\Delta = 0.8$ (black triangles) and $\lambda_\Delta = 2$ (orange squares). The blue circles denote the simulated curve for the equivalent standard SIS model ($\lambda_\Delta = 0$), which does not consider higher order effects. For $\lambda_\Delta = 2$ a bi-stable region appears, where healthy and endemic states co-exist.

orange lines): in this parameter region, the final state depends on the initial density of infectious nodes ρ_0 .

The simplicial complexes used in these simulations correspond to various social contexts and different densities of 1- and 2-simplices, and yield a similar phenomenology. These empirical structures however exhibit distributions of generalized degrees that are not well peaked around their average values (see Supplementary Note 1), and do not allow us to systematically explore size effects. To better understand the phenomenology of the simplicial contagion model, we thus now explore its behaviour on synthetic simplicial complexes with controlled properties.

Simplicial contagion on synthetic simplicial complexes. A range of models for random simplicial complexes have been proposed so far, starting from the exponential random simplicial complex, the growing and generalized canonical ensemble^{46–48} and the simplicial configuration models⁴⁹ to the simplicial activity driven model⁵⁰ generalizing the activity driven temporal network model⁵¹. While these yield Erdős-Rényi-like models^{52,53} of arbitrary complexity, here we are interested in models generating simplicial complexes with simplices of different dimension in which we can control and tune the expected local connectivity, e.g. the number of edges and “full” triangles a node belongs to. We therefore propose a new model to construct random simplicial complexes, the RSC model, which allows us to maintain the average degree of the nodes, $\langle k_1 \rangle$, fixed, while varying at the same time the expected number of “full” triangles (2-simplices) $\langle k_\Delta \rangle$ incident on a node. The RSC model of dimension D has $D + 1$ parameters, namely the number of vertices N and D probabilities $\{p_1, \dots, p_k, \dots, p_D\}$, $p_k \in [0, 1]$, which control for the cre-

ation of k -simplices up to dimension D . For the purpose of this study we limit the RSC model to $D = 2$, which restricts the set of required parameters to (N, p_1, p_2) , but the procedure could easily be extended to larger D . The model works as follows. We first create 1-simplices (links) as in the Erdős-Rényi model⁵⁴, by connecting any pair (i, j) of vertices with probability p_1 . Similarly, 2-simplices are then created by connecting any triplet (i, j, k) of vertices with probability $p_2 \equiv p_\Delta$. Notice that simplicial complexes built in this way are radically different from the clique complexes obtained from Erdős-Rényi graphs⁵², in which every subset of nodes forming a clique is automatically “promoted” to a simplex. Contrarily, in a simplicial complex generated by the RSC model proposed here, a 2-simplex (i, j, k) does not come from the promotion of an “empty” triangle composed by three 1-simplices (i, j) , (j, k) , (k, i) to a “full triangle” (i, j, k) . This also means that the model allows for the presence of $(k + 1)$ -cliques that are not considered k -simplices, therefore it is able generate simplicial complexes having both “empty” and “full” triangles, respectively encoding three 2-body interactions and one 3-body interactions (as for instance in Fig. 1b). The expected average numbers of 1- and 2-simplices incident on a node, noted $\langle k \rangle$ and $\langle k_\Delta \rangle$, are easy to calculate (see Methods). Therefore, for any given size N , we can produce simplicial complexes having desired values of $\langle k \rangle$ and $\langle k_\Delta \rangle$ by appropriately tuning p_1 and p_Δ . More details about the construction of the model and the tuning of the parameters are provided in the “Methods” section, while the agreement between the expected values of $\langle k \rangle$ and $\langle k_\Delta \rangle$ with the empirical averages obtained from different realizations of the model is discussed in Supplementary Note 1.

We simulate the SCM over a RSC created with the procedure described above, with $N = 2000$ nodes, $\langle k \rangle \simeq 20$ and $\langle k_\Delta \rangle \simeq 6$. As for the real-world simplicial complexes, we start with

a seed of ρ_0 infectious nodes placed at random and we compute the average stationary density of infectious ρ^* by averaging over different runs, each one using a different instance of the RSC model. Results are shown in Fig.3a, where the average fraction of infected nodes, as obtained by the simulations, is plotted as a function of the rescaled infectivity $\lambda = \beta\langle k \rangle$ for a ($D = 2$) SCM with $\lambda_\Delta = 0.8$ (white squares), $\lambda_\Delta = 2.5$ (filled blue circles) and $\lambda_\Delta = 0$ (light blue circles).

Despite the very different properties of the underlying structure, the dynamics of the SCM on the RSC is very similar to the one observed on the real-world simplicial complexes. For $\lambda_\Delta = 0.8$ the model behaves similarly to a simple contagion model ($\lambda_\Delta = 0$), with a continuous transition at $\lambda^c = 1$, the well-know epidemic threshold of the standard SIS model on homogeneous networks. When a higher value of λ_Δ is considered ($\lambda_\Delta = 2.5$), the epidemic can be sustained below $\lambda^c = 1$, and both an epidemic-free and an endemic states are present in the region $\lambda^c < \lambda < 1$, with appearance of a hysteresis loop (see the filled blue circles in Fig. 3a). In this region, we obtain $\rho(t \rightarrow \infty) = 0$ for $\rho(t = 0) = 0.01$, while $\rho(t \rightarrow \infty) > 0$ for $\rho(t = 0) = 0.4$. The size-dependence of the hysteresis loop is shown in Supplementary Note 2 to be very small. The dependency from the initial conditions is also further illustrated in Fig. 3b, in which the temporal dynamics of single runs are shown. The various curves show how the density of infected nodes $\rho(t)$ evolves when initial seeds of infected nodes of different sizes are considered. Each color corresponds to a different value of ρ_0 , with brighter colors representing higher initial densities of infected individuals. The figure clearly shows the presence of a threshold value for ρ_0 , such that $\rho(t)$ goes to the absorbing state $\rho(t) = 0$ if ρ_0 is smaller than the threshold, and to a non-trivial steady state if the initial density is above the threshold.

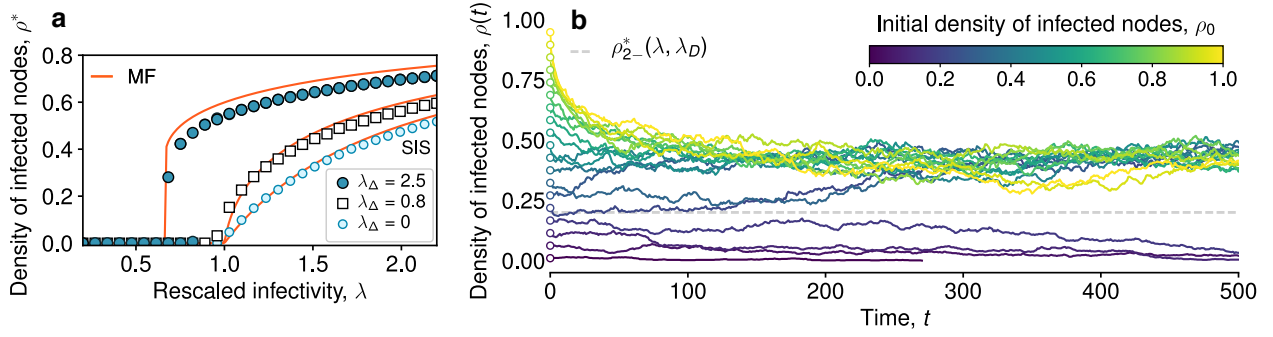


Figure 3: **SCM of order $D = 2$ on a synthetic random simplicial complex (RSC).** The RSC is generated with the procedure described in this manuscript, with parameters $N = 2000$, p_1 and p_Δ tuned in order to produce a simplicial complex with $\langle k \rangle \sim 20$ and $\langle k_\Delta \rangle \sim 6$. **a** The average fraction of infected obtained by means of numerical simulations is plotted against the rescaled infectivity $\lambda = \beta \langle k \rangle / \mu$ for $\lambda_\Delta = 0.8$ (white squares) and $\lambda_\Delta = 2.5$ (filled blue circles). The light blue circles give the numerical results for the standard SIS model ($\lambda_\Delta = 0$) that does not consider higher order effects. The red lines correspond to the analytical mean field solution described by Eq. (3). For $\lambda_\Delta = 2.5$ we observe a discontinuous transition with the formation of a bistable region where healthy and endemic states co-exist. **b** Effect of the initial density of infected nodes, shown by the temporal evolution of the densities of infectious nodes (a single realization is shown for each value of the initial density). The infectivity parameters are set within the range in which we observe a bistable region ($\lambda = \beta \langle k \rangle / \mu = 0.75$, $\lambda_\Delta = \beta_\Delta \langle k_\Delta \rangle / \mu = 2.5$). Different curves - and different colors - correspond to different values for the initial density of infectious nodes $\rho_0 \equiv \rho(0)$. The dashed horizontal line corresponds to the unstable branch ρ_{2-}^* of the mean field solution given by Eq. 4, which separates the two basins of attraction.

Mean field approach. In order to study more extensively this phenomenology as λ_Δ and λ vary, and to further characterize the discontinuous transition, we consider a mean field (MF) description of the SCM, under a homogeneous mixing hypothesis⁵⁵. Given the set of infection probabilities $B \equiv \{\beta_\omega, \omega = 1, \dots, D\}$ and a recovery probability μ , we assume the independence between the states $x_i(t)$ and $x_j(t) \forall i, j \in \mathcal{V}$, and we write a MF expression for the temporal evolution of the density of infected nodes $\rho(t)$ as:

$$d_t \rho(t) = -\mu \rho(t) + \sum_{\omega=1}^D \beta_\omega \langle k_\omega \rangle \rho^\omega(t) [1 - \rho(t)] \quad (1)$$

where, for each $\omega = 1, \dots, D$, $k_\omega(i) = k_{\omega,0}(i)$ is the generalized (simplicial) degree of a 0-dimensional face (node i), i. e., the number of ω -dimensional simplices incident to the node i ^{47,48}, and $\langle k_\omega \rangle$ is its average over all the nodes $i \in \mathcal{V}$. With this approximation we assume that the local connectivity of the nodes is well described by globally averaged properties, such as the average generalized degree. We can immediately check that in the case $D = 1$ we recover the standard MF equation for the SIS model, which leads to the well known stationary state solutions $\rho_1^{*[D=1]} = 0$ and $\rho_2^{*[D=1]} = 1 - \mu/(\beta \langle k \rangle)$. The absorbing state $\rho_1^{*[D=1]} = 0$ is the only solution for $\beta \langle k \rangle / \mu < 1$, i.e., below the epidemic threshold. When $\beta \langle k \rangle / \mu > 1$, this state becomes unstable while the solution $\rho_2^{*[D=1]}$ becomes a stable fixed point of the dynamics. The transition between these two regimes is continuous at $\beta \langle k \rangle / \mu = 1$.

Let us now focus on a more interesting but still analytically tractable case in which we extend the contagion dynamics up to dimension $D = 2$, so that Eq. (1) reads:

$$d_t \rho(t) = -\mu \rho(t) + \beta \langle k \rangle \rho(t) [1 - \rho(t)] + \beta_\Delta \langle k_\Delta \rangle \rho^2(t) [1 - \rho(t)] \quad (2)$$

where $\langle k_\Delta \rangle \equiv \langle k_2 \rangle$. By defining as before $\lambda = \beta \langle k \rangle / \mu$ and $\lambda_\Delta = \beta_\Delta \langle k_\Delta \rangle / \mu$, and by rescaling the time by μ , we can rewrite Eq. (2) as:

$$d_t \rho(t) = -\rho(t)(\rho(t) - \rho_{2+}^*)(\rho(t) - \rho_{2-}^*), \quad (3)$$

where ρ_{2+}^* and ρ_{2-}^* are the solutions of the second order equation $1 - \lambda(1 - \rho) - \lambda_\Delta \rho(1 - \rho) = 0$.

We thus obtain:

$$\rho_{2\pm}^* = \frac{\lambda_\Delta - \lambda \pm \sqrt{(\lambda - \lambda_\Delta)^2 - 4\lambda_\Delta(1 - \lambda)}}{2\lambda_\Delta}. \quad (4)$$

The steady state equation $d_t \rho(t) = 0$ has thus up to three solutions in the acceptable range $\rho \in [0, 1]$. The solution $\rho_1^* = 0$ corresponds to the usual absorbing epidemic-free state, in which all the individuals recover and the spreading dies out. A careful analysis of the stability of this state and of the two other solutions ρ_{2+}^* and ρ_{2-}^* is however needed to fully characterize the phase diagram of the system.

Let us first consider the case $\lambda_\Delta \leq 1$. It is possible to show that ρ_{2-}^* , when it is real-valued, is always negative, i.e., it is not an acceptable solution. Moreover, ρ_{2+}^* is positive for $\lambda > 1$ and negative for $\lambda < 1$. In the regime $\lambda_\Delta \leq 1$ therefore:

- if $\lambda < 1$, the only acceptable solution to $d_t \rho(t) = 0$ is $\rho_1^* = 0$;
- for $\lambda > 1$, since $\rho_{2-}^* < 0$ and $\rho_{2+}^* > 0$, Eq. (3) shows that $d_t \rho(t)$ is positive at small $\rho(t)$: the absorbing state $\rho_1^* = 0$ is thus unstable and the solution ρ_{2+}^* is stable. As $\rho_{2+}^* = 0$ for $\lambda = 1$, the transition at the epidemic threshold $\lambda = 1$ is continuous.

In conclusion, when $\lambda_\Delta \leq 1$, the transition is similar to the one of the standard SIS model with $\lambda_\Delta = 0$.

Let us now consider the case of $\lambda_\Delta > 1$. Then, for $\lambda < \lambda^c = 2\sqrt{\lambda_\Delta} - \lambda_\Delta$, both ρ_{2+}^* and ρ_{2-}^* are outside the real domain, and the only steady state is the absorbing one $\rho_1^* = 0$. Note that $\lambda^c < 1$, since $\lambda_\Delta > 1$. For $\lambda > \lambda^c$, we thus have two possibilities to consider:

- if $\lambda > 1$, we can show that $\rho_{2-}^* < 0 < \rho_{2+}^*$. Equation (3) shows then that, for small $\rho(t)$, $d_t\rho(t) > 0$: as above, the absorbing state $\rho_1^* = 0$ is unstable and the density of infectious nodes tends to ρ_{2+}^* in the large time limit;
- if instead $\lambda^c < \lambda < 1$, we obtain that $0 < \rho_{2-}^* < \rho_{2+}^*$. Then, still from Eq. (3), we obtain that $d_t\rho(t) < 0$ for $\rho(t)$ between 0 and ρ_{2-}^* , and that $d_t\rho(t) > 0$ for $\rho(t)$ between ρ_{2-}^* and ρ_{2+}^* . As a result, both $\rho_1^* = 0$ and ρ_{2+}^* are stable steady states of the dynamics, while ρ_{2-}^* is an unstable solution. Most interestingly, the long time limit of the dynamics depends then on the initial conditions. Indeed, if the initial density of infectious nodes, $\rho(t=0)$, is below ρ_{2-}^* , the short time derivative of $\rho(t)$ is negative, so that the density of infectious nodes decreases and the system tends to the absorbing state: $\rho(t) \xrightarrow[t \rightarrow \infty]{} 0$. On the other hand, if the initial density $\rho(t=0)$ is large enough (namely, larger than ρ_{2-}^*), the dynamical evolution Eq. (3) pushes the density towards the value ρ_{2+}^* , i.e. $\rho(t) \xrightarrow[t \rightarrow \infty]{} \rho_{2+}^*$. Since $\rho_{2+}^* > 0$, the transition at λ_c is discontinuous.

We illustrate these results by showing in Fig. 4a the solutions ρ_1^* , ρ_{2+}^* and ρ_{2-}^* as a function of

λ and for different values of λ_Δ . The vertical line corresponds to the standard epidemic threshold for the SIS model ($\lambda_\Delta = 0$). Dashed lines depict unstable branches, as given by ρ_{2-}^* . We emphasize again two important points. First, for $\lambda_\Delta > 1$ we observe a discontinuous transition at $\lambda^c = 2\sqrt{\lambda_\Delta} - \lambda_\Delta$, instead of the usual continuous transition at the epidemic threshold. Second, for $\lambda^c < \lambda < 1$ the final state depends on the initial density of infectious nodes, as described above: the absorbing state $\rho_1^* = 0$ is reached if the initial density $\rho(t = 0)$ is below the unstable steady state value ρ_{2-}^* ; on the contrary, if $\rho(t = 0)$ is above this value, the system tends to a finite density of infectious nodes equal to ρ_{2+}^* . In other words, a critical mass is needed to reach the endemic state, reminding of the recently observed minimal size of committed minorities required to initiate social changes ⁵⁶.

Figure 4b is a two-dimensional phase diagram showing ρ_{2+}^* for different values of λ and λ_Δ . Lighter colours correspond to higher values of the stationary density of infectious nodes, while the dashed vertical line corresponds to the epidemic threshold of the standard (without higher order effects) SIS model, namely $\lambda = 1$. For $\lambda_\Delta \leq 1$ (below the dashed horizontal line) the transition as λ crosses 1 is seen to be continuous, while, for $\lambda_\Delta > 1$, the transition is clearly discontinuous along the curve $\lambda^c = 2\sqrt{\lambda_\Delta} - \lambda_\Delta$ (dash-dotted line). The analytical values of ρ_{2+}^* are also reported as continuous red lines in Figure 3a and compared to the results of the simulations, showing in this way the accuracy of the mean field approach just described. In addition, Figure 3b shows that the unstable solution ρ_{2-}^* accurately separates the two basins of attractions for the dynamics, i.e., it defines the critical initial density of infected ρ_0 that determines whether the long term dynamics reaches the healthy state or the endemic one. Notice that the mean field approach is in fact able to

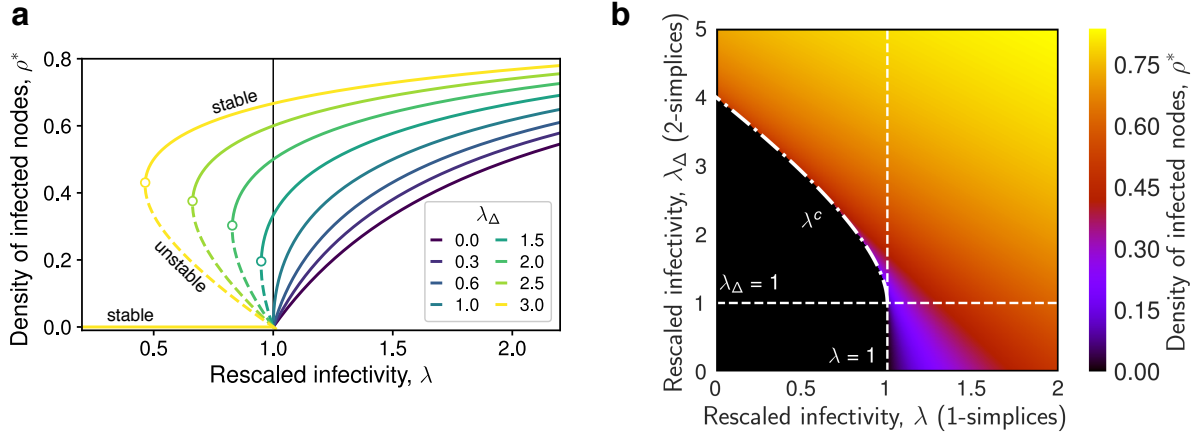


Figure 4: **Phase diagram of the SCM of order $D = 2$ in mean field approximation.** **a** The stationary solutions ρ^* given by Eq. (4) are plotted as a function of the rescaled link infectivity $\lambda = \beta\langle k \rangle/\mu$. Different curves correspond to different values of the triangle infectivity $\lambda_\Delta = \beta_\Delta\langle k_\Delta \rangle/\mu$. Continuous and dashed lines correspond to stable and unstable branches respectively, while the vertical line denotes the epidemic threshold $\lambda^c = 1$ in the standard SIS model that does not consider higher order effects. For $\lambda_\Delta \leq 1$ the higher order interactions only contribute to an increase in the density of infected individuals in the endemic state, while they leave the threshold unchanged. Conversely, when $\lambda_\Delta > 1$ we observe a shift of the epidemic threshold, and a change in the type of transition, which becomes discontinuous. **b** Heatmap of the stationary solution ρ^* given by Eq. (4) as a function of the rescaled infectivities $\lambda = \beta\langle k \rangle/\mu$ and $\lambda_\Delta = \beta_\Delta\langle k_\Delta \rangle/\mu$. The black area corresponds to the values of $(\lambda, \lambda_\Delta)$ such that the only stable solution is $\rho_1^* = 0$. The dashed vertical line corresponds to $\lambda = 1$, the epidemic threshold of the standard SIS model without higher order effects. The dash-dotted line represents the points $(\lambda^c, \lambda_\Delta)$, with $\lambda^c = 2\sqrt{\lambda_\Delta} - \lambda_\Delta$, where the system undergoes a discontinuous transition.

correctly capture both the position of the thresholds and the discontinuous nature of the transition for the SCM with $\lambda_\Delta > 1$.

We finally note that, while a general solution for general D with arbitrary parameters $\{\beta_\omega\}$ remains out of reach, it is possible to show that the phenomenology obtained for $D = 2$ is also observed for specific cases with $D \geq 3$. We consider indeed in the Supplementary Note 3 two cases: $D = 3$ with $\beta_2 = 0$ and general $D > 3$ with $\beta_1 = \dots = \beta_{D-1} = 0$. In both cases, we show the appearance of a discontinuous transition in the regime where the simple contagion β_1 is below threshold (i.e., $\beta_1 \langle k \rangle < \mu$): similarly to the case $D = 2$, this transition occurs as β_D , which describes the rate of the high-order contagion process, increases.

Discussion. In summary, the simplicial model of contagion introduced in this work is able to capture the basic mechanisms and effects of higher-order interactions in social contagion processes. Our analytical results were derived in a mean field approximation and indeed quantitatively compared to the nondescript simplicial complexes obtained in our random simplicial complex model (basically ER simplicial complexes). However, the framework we have introduced is very general and the phenomenology robust, as seen from the results obtained on empirical data sets. It would be interesting to investigate the SCM on more general simplicial complexes with for instance heterogeneous generalized degree distribution or with community structures, and to consider simplicial complexes with emergent properties such as hyperbolic geometry⁵⁷, or temporally evolving simplicial complexes⁵⁰. Furthermore, given that the SCM can be mapped on a model with hypergraphs if the hyperedges of different types are carefully chosen, it would be interesting to study

the behavior of complex contagion processes on more general classes of hypergraphs^{58,59}. Finally, we hope that the idea will be extended from spreading processes to other dynamical systems, for instance to Kuramoto-like models with higher-order terms. Developing and studying such systems might allow to better take into account higher-order dynamical effects in real data-driven models.

Methods

Data description and processing. We consider four data sets of face-to-face interactions collected in different social contexts: a workplace (InVS15)⁶⁰, a conference (SFHH)⁶¹, a hospital (LH10)⁶² and a high school (Thiers13)⁶³. In each case face-to-face interactions have been measured with a temporal resolution of 20 seconds. We first aggregated the data by using a temporal window of $\Delta t = 5$ minutes, and computed all the maximal cliques that appear. Since we limit our study to the case $D = 2$, we need to produce a clique complex formed by 1- and 2-simplices. Therefore, we considered all the 2- and 3-cliques and weight them according to their frequency. Note that while higher-dimensional cliques are not included in the final simplicial complex, their sub-cliques up to size 3 are considered in the counting. We then retained 20% of the simplices with the largest number of appearances. The thresholded simplicial complexes obtained in this way are those used in Supplementary Figure 6. Their connectivity properties are summarised in Table 1.

To reduce finite size effects, we augmented the thresholded simplicial complexes as follows: for each data set we extracted the list of sizes of the maximal simplices, also called facets, and the list of pure simplicial degrees of nodes. We then duplicated these lists five times and used the extended lists as input for the simplicial configuration model, described in Ref.⁴⁹. The outputs of

Dataset	Context	$\langle k \rangle$	$\langle k_\Delta \rangle$	$\langle k \rangle^{\text{aug}}$	$\langle k_\Delta \rangle^{\text{aug}}$
InVS15	Workplace	16.9	7.0	21.0	7.0
SFHH	Conference	15.0	7.6	21.6	7.7
LH10	Hospital	19.1	17.1	25.7	17.5
Thiers13	High school	20.1	10.9	32.0	11.1

Table 1: Average generalized degree of the four real-world simplicial complexes constructed from the considered data sets (before and after the data augmentation).

this procedure are simplicial complexes with the same statistical properties as the input complex but of significantly larger size. We used these augmented complexes as substrates for the simulations shown in Figure 2.

Construction of random simplicial complexes. The random simplicial complex (RSC) model produces simplicial complexes of dimension $D = 2$ as follows. Given a set \mathcal{V} of N vertices we connect any two nodes $i, j \in \mathcal{V}$ with probability $p_1 \in [0, 1]$, so that the average degree, at this stage, is $(N - 1)p_1$. Then, for any $i, j, k \in \mathcal{V}$, we add a 2-simplex (i, j, k) with probability $p_\Delta \in [0, 1]$. At this point each node has an average number $\langle k_\Delta \rangle = (N - 1)(N - 2)p_\Delta/2$ of incident 2-simplices that also contribute to increase the degree of the nodes. The exact contribution can be calculated by considering the different scenarios in which a 2-simplex (i, j, k) can be attached to a node i already having some links due to the first phase of the RSC construction. More precisely, the degree k_i of node i is incremented by 2 for each 2-simplex (i, j, k) such that neither the link (i, j) nor the link (i, k) are already present; this happens with probability $(1 - p_1)^2$. Analogously, if either the

link (i, j) is already present but not (i, k) , or vice-versa, the addition of the 2-simplex (i, j, k) increases the degree of i by 1. Since each case happens with the same probability $p_1(1 - p_1)$ the contribution is therefore $2p_1(1 - p_1)$. Overall, the degree k_i increases on average by $2(1 - p_1)$ for each 2-simplex attached to i . Finally, for $p_1, p_\Delta \ll 1$, we can thus write the expected average degree $\langle k \rangle$ as the sum of the two contributions coming from the links and the 2-simplices, namely $\langle k \rangle \approx (N - 1)p_1 + 2\langle k_\Delta \rangle(1 - p_1)$. For any given size N , we can thus produce simplicial complexes having desired values of $\langle k \rangle$ and $\langle k_\Delta \rangle$ by fixing p_1 and p_Δ as:

$$p_1 = \frac{\langle k \rangle - 2\langle k_\Delta \rangle}{(N - 1) - 2\langle k_\Delta \rangle} \quad (5a)$$

$$p_\Delta = \frac{2\langle k_\Delta \rangle}{(N - 1)(N - 2)}. \quad (5b)$$

1. Albert, R. & Barabási, A.-L. Statistical mechanics of complex networks. *Rev. Mod. Phys.* **74**, 47 (2002).
2. Latora, V., Nicosia, V. & Russo, G. *Complex Networks: Principles, Methods and Applications* (Cambridge University Press, 2017).
3. Radicchi, F. & Arenas, A. Abrupt transition in the structural formation of interconnected networks. *Nat. Phys.* **9**, 717 (2013).
4. Porter, M. A. & Gleeson, J. P. *Dynamical systems on networks: A tutorial* (Springer, 2005).
5. Barrat, A., Barthelemy, M. & Vespignani, A. *Dynamical processes on complex networks* (Cambridge university press, 2008).

6. Pastor-Satorras, R., Castellano, C., Van Mieghem, P. & Vespignani, A. Epidemic processes in complex networks. *Rev. Mod. Phys.* **87**, 925 (2015).
7. Valente, T. W. Network models of the diffusion of innovations. *Comp. Math. Org. Th.* **2**, 163–164 (1996).
8. Cowan, R. & Jonard, N. Network structure and the diffusion of knowledge. *J. Econ. Dyn. Control* **28**, 1557–1575 (2004).
9. Iacopini, I., Milojević, S. & Latora, V. Network dynamics of innovation processes. *Phys. Rev. Lett.* **120**, 048301 (2018).
10. Watts, D. J. & Dodds, P. S. Influentials, networks, and public opinion formation. *J. Consum. Res.* **34**, 441–458 (2007).
11. Centola, D. & Macy, M. Complex contagions and the weakness of long ties. *Americ. J. Sociol.* **113**, 702–734 (2007).
12. Guilbeault, D., Becker, J. & Centola, D. Complex contagions: A decade in review. In *Complex Spreading Phenomena in Social Systems*, 3–25 (Springer, 2018).
13. Centola, D. The spread of behavior in an online social network experiment. *Science* **329**, 1194–1197 (2010).
14. Ugander, J., Backstrom, L., Marlow, C. & Kleinberg, J. Structural diversity in social contagion. *Pro. Natl. Acad. Sci. U.S.A.* 201116502 (2012).

15. Weng, L., Flammini, A., Vespignani, A. & Menczer, F. Competition among memes in a world with limited attention. *Sci. Rep.* **2**, 335 (2012).
16. Karsai, M., Iniguez, G., Kaski, K. & Kertész, J. Complex contagion process in spreading of online innovation. *J. R. Soc. Interface* **11**, 20140694 (2014).
17. Mønsted, B., Sapieżyński, P., Ferrara, E. & Lehmann, S. Evidence of complex contagion of information in social media: An experiment using twitter bots. *PLoS One* **12**, e0184148 (2017).
18. Watts, D. J. A simple model of global cascades on random networks. *Pro. Natl. Acad Sci. U.S.A.* **99**, 5766–5771 (2002).
19. Melnik, S., Ward, J. A., Gleeson, J. P. & Porter, M. A. Multi-stage complex contagions. *Chaos* **23**, 013124 (2013).
20. Ruan, Z., Iniguez, G., Karsai, M. & Kertész, J. Kinetics of social contagion. *Phys. Rev. Lett.* **115**, 218702 (2015).
21. Czaplicka, A., Toral, R. & San Miguel, M. Competition of simple and complex adoption on interdependent networks. *Phys. Rev. E* **94**, 062301 (2016).
22. Cozzo, E., Banos, R. A., Meloni, S. & Moreno, Y. Contact-based social contagion in multiplex networks. *Phys. Rev. E* **88**, 050801 (2013).
23. Hodas, N. O. & Lerman, K. The simple rules of social contagion. *Sci. Rep.* **4**, 4343 (2014).

24. Herrera, M., Armelini, G. & Salvaj, E. Understanding social contagion in adoption processes using dynamic social networks. *PLoS One* **10**, e0140891 (2015).
25. O’Sullivan, D. J., O’Keeffe, G. J., Fennell, P. G. & Gleeson, J. P. Mathematical modeling of complex contagion on clustered networks. *Front. Phys.* **3**, 71 (2015).
26. Tuzón, P., Fernández-Gracia, J. & Eguíluz, V. M. From continuous to discontinuous transitions in social diffusion. *Front. Phys.* **6**, 21 (2018).
27. Hatcher, A. *Algebraic topology* (2002).
28. Salnikov, V., Cassese, D. & Lambiotte, R. Simplicial complexes and complex systems. *European Journal of Physics* **40**, 014001 (2018).
29. Kee, K. F., Sparks, L., Struppa, D. C. & Mannucci, M. Social groups, social media, and higher dimensional social structures: A simplicial model of social aggregation for computational communication research. *Communication Quarterly* **61**, 35–58 (2013).
30. Aleksandrov, P. S. *Combinatorial topology*, vol. 1 (Courier Corporation, 1998).
31. Sizemore, A. E., Phillips-Cremins, J., Ghrist, R. & Bassett, D. S. The importance of the whole: topological data analysis for the network neuroscientist. *arXiv preprint arXiv:1806.05167* (2018).
32. Carlsson, G. Topology and data. *Bull. Am. Math. Soc.* **46**, 255–308 (2009).
33. Petri, G., Sciamiero, M., Donato, I. & Vaccarino, F. Topological strata of weighted complex networks. *PLoS One* **8**, e66506 (2013).

34. Sizemore, A., Giusti, C. & Bassett, D. S. Classification of weighted networks through mesoscale homological features. *J. Comp. Net.* **5**, 245–273 (2016).
35. Kartun-Giles, A. P. & Bianconi, G. Beyond the clustering coefficient: A topological analysis of node neighbourhoods in complex networks. *arXiv preprint arXiv:1901.10978* (2019).
36. Petri, G. *et al.* Homological scaffolds of brain functional networks. *J. Royal Soc. Interface* **11**, 20140873 (2014).
37. Lord, L.-D. *et al.* Insights into brain architectures from the homological scaffolds of functional connectivity networks. *Front. Syst. Neurosci.* **10**, 85 (2016).
38. Lee, H., Kang, H., Chung, M. K., Kim, B.-N. & Lee, D. S. Persistent brain network homology from the perspective of dendrogram. *IEEE Trans. Med. Imaging.* **31**, 2267–2277 (2012).
39. Sizemore, A. E. *et al.* Cliques and cavities in the human connectome. *J. Comp. Neurosci.* **44**, 115–145 (2018).
40. Estrada, E. & Ross, G. J. Centralities in simplicial complexes. applications to protein interaction networks. *J. Theor. Biol.* **438**, 46–60 (2018).
41. Sizemore, A. E., Karuza, E. A., Giusti, C. & Bassett, D. S. Knowledge gaps in the early growth of semantic networks. *arXiv preprint arXiv:1709.00133* (2017).
42. Patania, A., Petri, G. & Vaccarino, F. The shape of collaborations. *EPJ Data Sci.* **6**, 18 (2017).
43. Berge, C. *Hypergraphs: combinatorics of finite sets*, vol. 45 (Elsevier, 1984).

44. Ghoshal, G., Zlatić, V., Caldarelli, G. & Newman, M. Random hypergraphs and their applications. *Phys. Rev. E* **79**, 066118 (2009).
45. SocioPatterns Collaboration. <http://www.sociopatterns.org/> (Accessed Dec 2018).
46. Zuev, K., Eisenberg, O. & Krioukov, D. Exponential random simplicial complexes. *J. Phys. A* **48**, 465002 (2015).
47. Courtney, O. T. & Bianconi, G. Generalized network structures: The configuration model and the canonical ensemble of simplicial complexes. *Phys. Rev. E* **93**, 062311 (2016).
48. Courtney, O. T. & Bianconi, G. Weighted growing simplicial complexes. *Phys. Rev. E* **95**, 062301 (2017).
49. Young, J.-G., Petri, G., Vaccarino, F. & Patania, A. Construction of and efficient sampling from the simplicial configuration model. *Phys. Rev. E* **96**, 032312 (2017).
50. Petri, G. & Barrat, A. Simplicial activity driven model. *Phys. Rev. Lett.* **121**, 228301 (2018).
51. Perra, N., Gonçalves, B., Pastor-Satorras, R. & Vespignani, A. Activity driven modeling of time varying networks. *Sci. Rep.* **2**, 469 (2012).
52. Kahle, M. Topology of random clique complexes. *Discrete Mathematics* **309**, 1658–1671 (2009).
53. Costa, A. & Farber, M. Random simplicial complexes. In *Configuration Spaces*, 129–153 (Springer, 2016).

54. Erdos, P. & Rényi, A. On the evolution of random graphs. *Publ. Math. Inst. Hung. Acad. Sci* **5**, 17–60 (1960).
55. Kiss, I. Z., Miller, J. C., Simon, P. L. *et al.* Mathematics of epidemics on networks. *Cham: Springer* (2017).
56. Centola, D., Becker, J., Brackbill, D. & Baronchelli, A. Experimental evidence for tipping points in social convention. *Science* **360**, 1116–1119 (2018).
57. Bianconi, G. & Rahmede, C. Emergent hyperbolic network geometry. *Sci. Rep.* **7**, 41974 (2017).
58. Bodó, Á., Katona, G. Y. & Simon, P. L. SIS epidemic propagation on hypergraphs. *B. Math. Biol.* **78**, 713–735 (2016).
59. Lanchier, N. & Neuffer, J. Stochastic dynamics on hypergraphs and the spatial majority rule model. *J. Stat. Phys* **151**, 21–45 (2013).
60. Génois, M. & Barrat, A. Can co-location be used as a proxy for face-to-face contacts? *EPJ Data Science* **7**, 11 (2018).
61. Isella, L. *et al.* What’s in a crowd? analysis of face-to-face behavioral networks. *J. Theor. Biol* **271**, 166–180 (2011).
62. Vanhems, P. *et al.* Estimating potential infection transmission routes in hospital wards using wearable proximity sensors. *PLoS One* **8**, e73970 (2013).

63. Mastrandrea, R., Fournet, J. & Barrat, A. Contact patterns in a high school: a comparison between data collected using wearable sensors, contact diaries and friendship surveys. *PLoS One* **10**, e0136497 (2015).

Data availability The SocioPatterns data sets were downloaded from <http://www.sociopatterns.org/datasets>.

Acknowledgements I. I. and V. L. acknowledge support from EPSRC Grant EP/N013492/1. I. I. acknowledges support from The Alan Turing Institute under the EPSRC Grant No. EP/N510129/1, and G. P. from ADnD Grant by Compagnia San Paolo.

Author contributions I.I., G.P., A.B. and V.L. designed the study. I.I. and G.P. performed the numerical analysis. I.I., G.P., A.B. and V.L. wrote the paper.

Competing interests The authors declare that they have no competing financial interests.

Correspondence Correspondence and requests for materials should be addressed to V.L. (email: v.latora@qmul.ac.uk).

Supplementary Information

“Simplicial models of social contagion”

Iacopini et al.

1 Generalized degree distributions of empirical and synthetic simplicial complexes

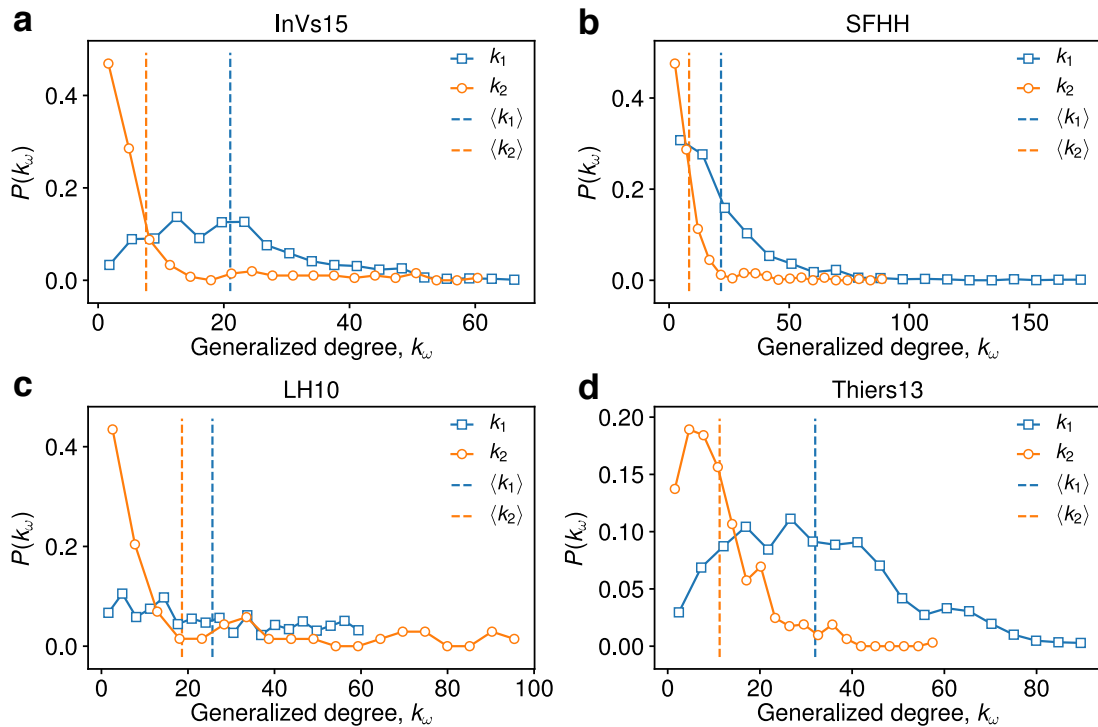


Figure 1: Generalised degree distributions of random simplicial complexes created from real world data sets (see the data processing method described in the “Methods” section of the main text). The four panels correspond to different social contexts, namely a workplace (InVS15), a conference (SFHH), a hospital (LH10) and a high school (Thiers13). The generalised degrees k_1 and $k_2 = k_\Delta$ denote respectively the number of 1-simplices (blue) and 2-simplices (orange) incident in a node. The vertical dashed lines indicate the corresponding average values.

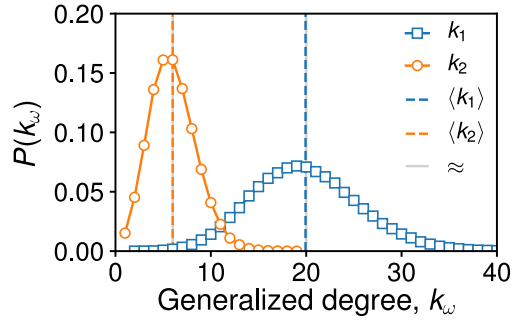


Figure 2: Generalised degree distributions of random simplicial complexes (RSC) generated by the model described in the main text. The generalised degrees k_1 and $k_2 = k_\Delta$ denote respectively the number of 1-simplices (blue) and 2-simplices (orange) incident in a node. The vertical lines compare the average values of $\langle k_1 \rangle$ and $\langle k_2 \rangle$ obtained from multiple realizations of the model (coloured dashed lines) with the approximated values (continuous grey lines) calculated as described in the main text.

2 Hysteresis and system size

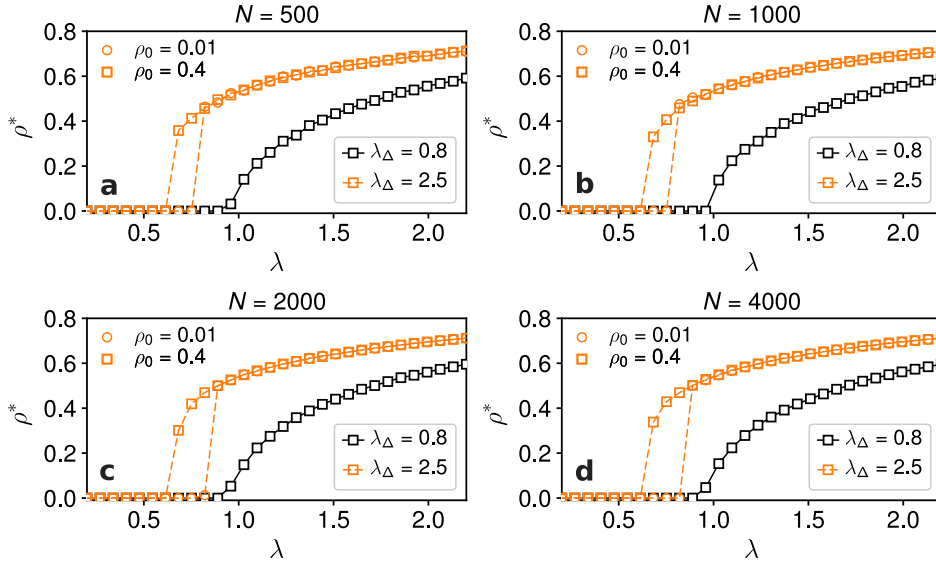


Figure 3: Numerical exploration of the finite size effects on the hysteresis for a SCM of order $D = 2$ on synthetic random simplicial complexes (RSC). The RSCs are generated with the procedure described in the main text, with parameters p_1 and p_{Δ} tuned in order to produce simplicial complexes with $\langle k \rangle \sim 20$ and $\langle k_{\Delta} \rangle \sim 6$. Different panels correspond to different system sizes, namely $N = 500, 1000, 2000$, and 4000 . Each panel shows the average stationary fraction of infected individuals plotted against the rescaled infectivity $\lambda = \beta \langle k \rangle / \mu$. The parameter $\lambda_{\Delta} = \beta_{\Delta} \langle k_{\Delta} \rangle / \mu$ is set to $\lambda_{\Delta} = 2.5$, which corresponds to the case in which we observe a discontinuous transition, with the formation of a bistable region where healthy and endemic states co-exist and a hysteresis appears. The two types of orange symbols correspond to two different values of the initial density of infected individuals for $\lambda_{\Delta} = 2.5$, namely $\rho_0 = 0.01$ (circles) and $\rho_0 = 0.4$ (squares). The case $\lambda_{\Delta} = 0.8$, in which we observe a continuous transition with no hysteresis, is shown for reference (black squares).

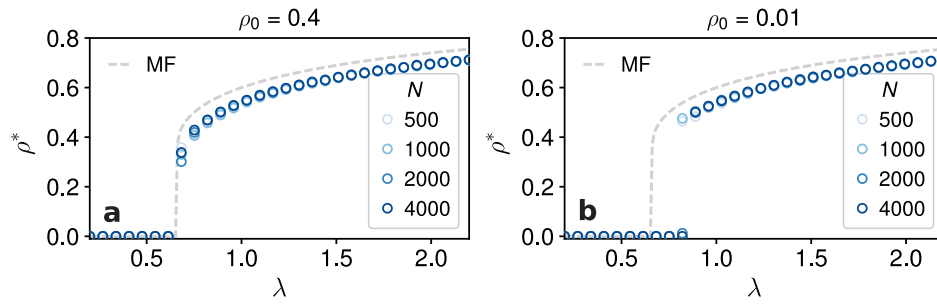


Figure 4: Numerical exploration of the finite size effects on the hysteresis for a SCM of order $D = 2$ on synthetic random simplicial complexes (RSC). The two panels refer to two different values of the initial density of infected individuals. The dashed line corresponds to the mean-field result.

3 Cases of higher dimensions

Case $D = 3$

Let us consider here a system with maximum dimension of simplices $D = 3$. In this case the model has three spreading parameters β_1 , $\beta_2 = \beta_\Delta$ and β_3 , and the evolution equation for $\rho(t)$ reads

$$d_t \rho(t) = -\mu \rho(t) + \beta \langle k \rangle \rho(t)(1 - \rho(t)) + \beta_2 \langle k_2 \rangle \rho(t)^2(1 - \rho(t)) + \beta_3 \langle k_3 \rangle \rho(t)^3(1 - \rho(t)). \quad (1)$$

Finding the roots of $d_t \rho(t) = 0$ yields a polynomial of degree 3, so it is possible to write these roots, corresponding to stable and unstable fixed points of the dynamics, as functions of the parameters of the model. The process is however lengthy and cumbersome, and depends moreover on three parameters, so that the representation of the whole phase diagram is not convenient.

As we want here simply to show that the phenomenology of the appearance of first order transitions obtained in the case $D = 2$, is also observed in higher dimensions, we restrict ourselves for simplicity to the case $\beta_\Delta = 0$, in which we will see that we can avoid writing the explicit solutions and resort instead to a graphical solution. This case corresponds to the hypothesis that contagion can occur only either through simple contagion or through cliques of size 4 in which 3 of the nodes are already infectious, and the evolution equation reduces to:

$$d_t \rho(t) = -\mu \rho(t) + \beta \langle k \rangle \rho(t)(1 - \rho(t)) + \beta_3 \langle k_3 \rangle \rho(t)^3(1 - \rho(t)). \quad (2)$$

Setting $\lambda = \beta \langle k \rangle / \mu$, $\lambda_3 = \beta_3 \langle k_3 \rangle / \mu$ and rescaling time by μ we obtain:

$$d_t \rho(t) = \rho(t)(1 - \rho(t)) \left(\lambda + \lambda_3 \rho^2 - \frac{1}{1 - \rho(t)} \right) \quad (3)$$

where we can define the functions $f_1(\rho) = \lambda + \lambda_3\rho^2$ and $f_2(\rho) = 1/(1 - \rho)$. The sign of the temporal evolution of the density of infectious is thus given by the sign of the difference between $f_1 - f_2$. Note that $\rho(t)$ is by definition between 0 and 1 so we need to consider f_1 and f_2 only between these limits. In this interval, f_1 is positive and increases monotonically from λ for $\rho = 0$ to $\lambda + \lambda_3$ for $\rho = 1$. Function f_2 is also positive and strictly increasing, with $f_2(0) = 1$ and f_2 diverging towards $+\infty$ as $\rho \rightarrow 1^-$. We also note that the equation $f_1(\rho) = f_2(\rho)$ yields a polynomial of degree 3, so it has at most 3 real roots.

Let us first consider the case $\lambda > 1$. Then at $\rho = 0$ we have $f_1 > f_2$, and as $\rho \rightarrow 1$, f_1 becomes smaller than f_2 . Therefore, at small ρ , $d_t\rho$ is positive and hence the state $\rho = 0$ is unstable. More in detail, there are two possibilities:

- either there is one single crossing point of f_1 and f_2 , at ρ^* . Then, $d_t\rho(t) > 0$ if $\rho(t) < \rho^*$ and $d_t\rho(t) < 0$ if $\rho(t) > \rho^*$: for any $\rho(t = 0) > 0$, the system goes to the stationary state $\rho(t \rightarrow \infty) = \rho^*$. This is similar to the usual SIS case with $\lambda_3 = 0$: the effect of a non-zero value of λ_3 is simply to shift the value of ρ^* .
- or there are three crossing points $\rho_1 < \rho_2 < \rho_3$. This occurs for certain combinations of values of λ and λ_3 . Then for $\rho(t) < \rho_1$, $d_t\rho(t) > 0$ so the absorbing state $\rho = 0$ is again unstable. The state ρ_2 is also seen to be unstable while there are two stable fixed points ρ_1 and ρ_3 : depending on the value of $\rho(t = 0)$, the system will converge to one of these values.

Hence, for $\lambda > 1$, the system always reaches a stationary state with a finite fraction of infectious

nodes, which in some regions of the (λ, λ_3) phase diagram, can depend on $\rho(t = 0)$.

Let us now consider the more interesting case $\lambda < 1$. Then $f_1(\rho) < f_2(\rho)$ both for $\rho = 0$ and as $\rho \rightarrow 1$. Hence $f_1 - f_2$ is negative both in 0 and 1, and either 0 or 2 of the roots of the equation $f_1(\rho) = f_2(\rho)$ are between 0 and 1. Hence, for $\rho \in [0, 1]$, either f_1 is always below f_2 , or the two functions intersect in 2 points that we call ρ_- and ρ_+ ($\rho_- < \rho_+$):

- in the former case ($f_1(\rho) < f_2(\rho) \forall \rho \in [0, 1]$), $d_t \rho(t)$ is always negative so the only stationary state is the absorbing one $\rho = 0$;
- in the latter case, $d_t \rho$ is positive for $\rho(t)$ between ρ_- and ρ_+ and negative else, so that
 - if $\rho(t = 0) < \rho_-$, $d_t \rho$ is negative, hence $\rho(t)$ decreases and the system converges to $\rho = 0$
 - if $\rho(t = 0) > \rho_+$, the system converges towards $\rho(t \rightarrow \infty) = \rho_+ > 0$.

At fixed $\lambda < 1$, the former case is obtained at small values of λ_3 , while the latter is obtained for λ_3 large enough. The situation is illustrated in Fig. 5 for $\lambda = 0.5$. At the transition $\lambda_3 = \lambda_3^c$ between these two cases, $\rho_- = \rho_+ > 0$ (the functions f_1 and f_2 are tangent in this point): the transition from $\rho(t \rightarrow \infty) = 0$ for $\lambda_3 < \lambda_3^c$ to $\rho(t \rightarrow \infty) = \rho_+$ (if $\rho(t = 0) > \rho_-$) for $\lambda_3 > \lambda_3^c$ is thus a discontinuous one, in a similar way to the case $D = 2$ discussed in the main text.

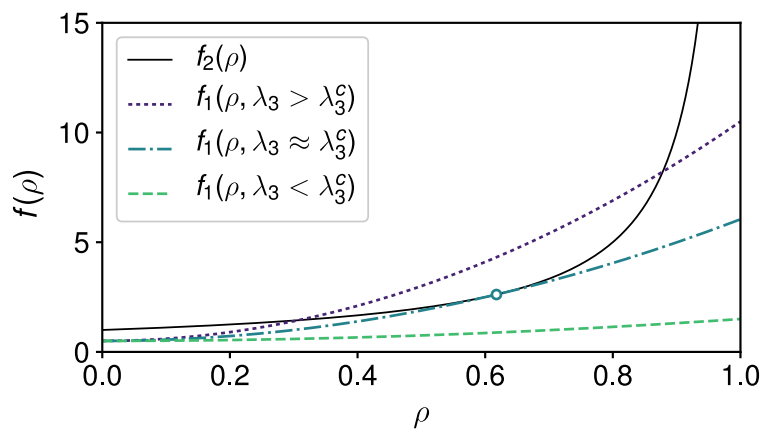


Figure 5: SCM of order $D = 3$, case $\lambda = 0.5$, $\lambda_2 = 0$: $f_1(\rho)$ for various λ_3 ($<$, \approx and $>$ λ_3^c), and $f_2(\rho)$. f_1 is below f_2 both at $\rho = 0$ and as $\rho \rightarrow 1$. The two curves therefore either do not cross (for $\lambda_3 < \lambda_3^c$), are tangent in $\rho_+ = \rho_-$ (for $\lambda_3 = \lambda_3^c$) or cross in two points ρ_- and ρ_+ (for $\lambda_3 > \lambda_3^c$).

General D , with $\beta_1 = \dots = \beta_{D-1} = 0$

For general D , there is no analytical solution for the stationary values of the density of infectious nodes. We show here however that, if we consider that contagion can occur only through cliques of size $D + 1$, i.e., if all spreading rates $\beta_1, \beta_2, \dots, \beta_{D-1}$ are null, there exists a discontinuous transition between the phase in which the spreading vanishes at low β_D and the phase in which $\rho(t \rightarrow \infty)$ is finite at large β_D .

The evolution equation for ρ reads

$$d_t \rho(t) = -\mu \rho(t) + \beta_D \langle k_D \rangle \rho(t)^D (1 - \rho(t)). \quad (4)$$

Defining $\lambda_D = \beta_D \langle k_D \rangle / \mu$ and rescaling time by μ we obtain

$$d_t \rho(t) = -\rho(t) \left[1 - \lambda_D \rho^{D-1}(t) (1 - \rho(t)) \right]. \quad (5)$$

Defining $F_D(\rho) = 1 - \lambda_D \rho^{D-1} (1 - \rho)$, we see that the sign of $d_t \rho(t)$ is opposite to the sign of $F_D(\rho(t))$, so that we need to study the sign of the function $F_D(\rho)$ for $\rho \in [0, 1]$ (as the density $\rho(t)$ is by definition between 0 and 1).

We have $F_D(0) = F_D(1) = 1$. Moreover, the derivative of F_D is

$$F'_D(\rho) = \lambda_D (D \rho^{D-1} - (D-1) \rho^{D-2}) = D \lambda_D \rho^{D-2} (\rho - (1 - 1/D)).$$

It is thus negative for $\rho < 1 - 1/D$ and positive for $\rho > 1 - 1/D$: F_D first decreases as ρ increases, reaches a minimum at $\rho = 1 - 1/D$ and then increases back to 1 as ρ increases to 1. We have thus two cases:

- if the minimum, $F_D(1 - 1/D)$, is positive, then $F_D(\rho) > 0$ for $\rho \in [0, 1]$: therefore, $d_t \rho(t)$ is always negative for any $\rho(t) > 0$: the density of infectious nodes can only decrease and the contagion-free state $\rho = 0$ is the only stable state.
- if instead $F_D(1 - 1/D) < 0$, then, as $F_D(0) = F_D(1) = 1$, by continuity the equation $F_D(\rho) = 0$ has two roots in $[0, 1]$, which we call ρ_- and ρ_+ ($\rho_- < \rho_+$). $F_D(\rho)$ is positive for $\rho \in [0, \rho_-)$ and $\rho \in (\rho_+, 1]$ and negative between the two roots. Therefore
 - if $\rho(t = 0) < \rho_-$, $d_t \rho(t = 0)$ is negative, hence $\rho(t)$ decreases and the system converges to $\rho = 0$
 - if $\rho(t = 0) > \rho_+$, the system converges towards $\rho(t \rightarrow \infty) = \rho_+ > 0$.

The condition to have $F_D(1 - 1/D) < 0$ and hence a non-trivial stationary state can be written simply as

$$1 - \lambda_D(1 - 1/D)^{D-1}(1/D) < 0$$

i.e.,

$$\lambda_D > \lambda_D^c = \frac{D^D}{(D-1)^{D-1}}.$$

Note that for $\lambda_D = \lambda_D^c$, $\rho_- = \rho_+ = 1 - 1/D$ is strictly positive, showing that the transition at λ_D^c is discontinuous.

This shows therefore that for $\beta_1 = \dots = \beta_{D-1} = 0$, we have the same phenomenology for any D as for the case $D = 2$ studied on the main text: a discontinuous transition occurs at $\lambda_D^c = \frac{D^D}{(D-1)^{D-1}}$ between an absorbing state $\rho = 0$ and a stationary state with a non-zero density of infectious individuals $\rho_+ > 0$.

4 Hypergraphs and simplicial complexes

Hypergraphs are a generalization of the concept of graphs in which the edges, called hyperedges, can join any number of vertices. Formally, a hypergraph \mathcal{H} is the pair of sets (V, E) , where V is a set of vertices, and the set of hyperedges E is a subset of the power set $P(V)$ of V . Simplicial complexes are therefore special kinds of hypergraphs, which contain all subsets of every hyperedge. A simplicial complex \mathcal{K} on the set of vertices V can indeed be seen as a hypergraph \mathcal{H} on V if the latter satisfies the extra requirement that, for each $\sigma \in E$, and for all $\nu \neq \emptyset$ such that $\nu \subseteq \sigma$, we also have $\nu \in E$. Such an extra requirement seems appropriate in the context of models of social interactions considered in our work, and it also turns useful to keep the model simple and amenable to analytical solution. However, the SCM can be straightforwardly extended to model the more general case of complex contagion processes on hypergraphs.

5 Results on empirical simplicial complexes without data augmentation

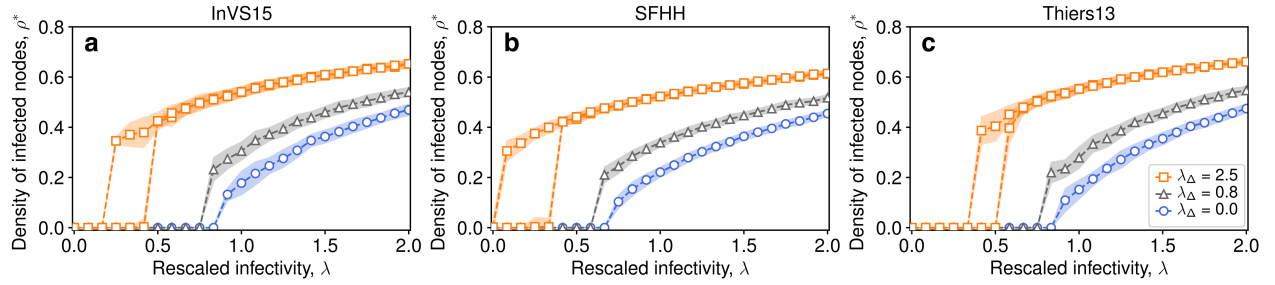


Figure 6: SCM of order $D = 2$ on real-world higher-order social structures without data augmentation. Simplicial complexes are constructed from high-resolution face-to-face contact data recorded in a workplace (a), a conference (b), and a high school (c). The average fraction of infected nodes in the stationary state obtained numerically is plotted against the rescaled infectivity $\lambda = \beta \langle k \rangle / \mu$ for $\lambda_{\Delta} = 0.8$ (black triangles) and $\lambda_{\Delta} = 2.5$ (orange squares). The blue circles denote the simulated curve for the standard SIS model ($\lambda_{\Delta} = 0$), which does not consider higher order effects. For $\lambda_{\Delta} = 2.5$ a bi-stable region appears, where healthy and endemic states co-exist.